ACS APPLIED ENERGY MATERIALS

www.acsaem.org Letter

Light Management in Bifacial Photovoltaics with Spectrally Selective Mirrors

Bryan M. Cote, Ian M. Slauch, Michael G. Deceglie, Timothy J Silverman, and Vivian E. Ferry*

Cite This: *ACS Appl. Energy Mater.* 2021, 4, 5397−5402 Read Online

ACCESS | Metrics & More | Article Recommendations | Supporting Information

ABSTRACT: Spectrally selective mirrors that simultaneously provide above-bandgap antireflection and sub-bandgap light rejection are tested for their ability to provide passive cooling to partially sub-bandgap transparent bifacial photovoltaics. The optical and thermal benefits of both idealized and real, low-complexity spectrally selective mirrors on single-axis tracking, bifacial PERC arrays under realistic conditions are tested via rigorous finite element simulations. Four- and six-layer mirror designs increased carrier generation beyond what traditional antireflection coatings can provide without the associated cell heating. Idealized mirrors were found to provide up to 2.4 °C of cooling when included on both air/glass interfaces of the bifacial module.

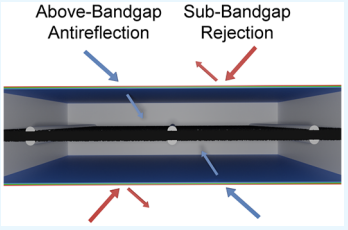

KEYWORDS: *bifacial photovoltaics, light management, cooling, antireflection coatings, photonic structures, solar energy*

Bifacial photovoltaics (bPVs) are expected to gain a significant market share over the next several years, driven by their increased power generation and comparable cost relative to monofacial photovoltaics (mPVs).[1−3] The rear face of a PERC solar cell can be readily opened to enable the collection of photons,[4] resulting in a 10%−30% increase in energy yield.[5] Placing bPVs in single-axis tracking arrays can further increase energy production and lower the levelized cost of energy.[3,6,7] Unfortunately, bPVs can also operate at hotter temperatures than mPVs:[8] monofacial Si PVs routinely operate 20−30 °C above ambient temperature,[9] and adding high fractions of rear irradiance can increase the operating temperature further. Elevated temperatures lead to an instantaneous efficiency decrease through a −0.3 to −0.4%/K temperature coefficient and reduce the operating lifetime of the module.[10] Numerous strategies[11] have been considered to provide thermal management for mPVs including water,[12] evaporative cooling,[13] phase change materials,[14] desiccants,[15] radiative cooling,[16] and selective reflectors.[17−20] However, many of these strategies may not be compatible with bPVs, and studies on the optical and thermal management of the rear side photons are needed. In this Letter, we investigate spectrally selective mirrors for light management in bifacial, single-axis tracking photovoltaics under realistic operating conditions.

The spectrally selective mirrors were designed to increase the power output by simultaneously increasing carrier generation via above-bandgap antireflection (optical benefit) and decreasing cell temperature via sub-bandgap reflection (thermal benefit),[18] as schematically depicted in Figure 1a. Much of the elevated operating temperature in Si modules arises from the parasitic absorption of sub-bandgap light, frequently in the back-contact of the cell. In monofacial modules, spectrally selective mirrors prevent sub-bandgap sunlight from entering the cell and reduce the operating temperature.[11,18,19] In a bifacial module, however, sub-bandgap light can also be transmitted; the addition of a spectrally selective mirror to the rear that reflects sub-bandgap light could also lead to detrimental trapping of infrared radiation. Therefore, it is unclear if the addition of a spectrally selective mirror on the rear face will actually decrease the operating temperature.

The test cell used in this report was a 20.6% efficient commercial bifacial PERC cell with 46% bifaciality (section S1, Figures S1−S3). The optical response of the test cell was modeled by using ray tracing simulations[21] that closely matched experimental reflection and transmission measurements (Figure S4). We used two different methods to calculate the optical and thermal benefits (sections S2−S4). Briefly, both methods start with a SMARTS2[22,23] integrated version of NREL's Bifacial View Factor Model[24] to generate time, wavelength, and angle of incidence resolved irradiance data on both faces of the single-axis tracking array over a typical meteorological year. These results where then either directly fed into a finite element model based on NREL's TOMCAT[11,25] or used in a simplified time-independent model analogous to a previously published method.[19] The simplified study discussed below and realistic mirror optimization utilized the time-independent model, while all other results were obtained with the more rigorous finite element simulations. The baseline for all optical and thermal

Received: May 1, 2021
Accepted: May 28, 2021
Published: June 2, 2021

https://doi.org/10.1021/acsaem.1c01236
ACS Appl. Energy Mater. 2021, 4, 5397−5402

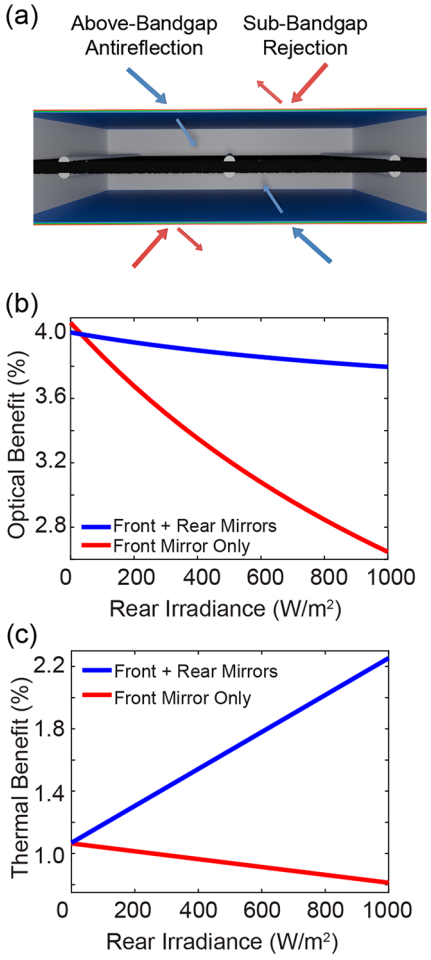

Figure 1. (a) Schematic of the bifacial module with spectrally selective mirrors on both air/glass interfaces. (b) Optical and (c) thermal benefits of an ideal spectrally selective mirror placed on either only the front or both air/glass interfaces with varying rear irradiance.

benefit calculations was an uncoated bifacial PERC module under identical conditions.

To gain initial insight into the optical and thermal benefit of this approach for bPVs, idealized spectrally selective mirrors were modeled on either the front only or both the front and rear air/glass interfaces of the test module. Ideal mirrors were defined as having unity transmission at wavelengths shorter than 1160 nm and unity reflection at longer wavelengths. In this simplified first test, AM1.5G spectral distributions[26] were normally incident on the front and rear faces of the module. The 1 sun standard irradiance of 1000 W/m^2 was held constant on the front while the irradiance incident on the rear face varied from 0 to 1000 W/m^2. The 1000 W/m^2 rear irradiance is significantly larger than the 130−140 W/m^2 expected under 1 sun test conditions,[27] but the simulations were extended to these high levels of rear irradiance to better highlight the physics of the system.

Figures 1b and 1c show that the addition of a spectrally selective mirror enhances the energy yield of the bifacial module relative to the unmirrored baseline module. The optical benefit in the case where a mirror is applied only to the front side decreases rapidly with increasing rear irradiance. The front mirror only provides antireflection to light incident on the front face, which becomes an increasingly small percentage of the overall irradiance incident on the module. The optical benefit decrease between the 0 and 1000 W/m^2 rear irradiance cases is significant but is notably not a factor of 2. This is due to the test cell's low bifaciality (46%), making the acceptance of rear side incident radiation less impactful than front side irradiance. When mirrors are applied to both faces, the optical benefit is better maintained, though a slight decrease is observed which is also attributed to low bifaciality.

The case of zero rear irradiance is of particular interest, where the front-only configuration has a larger optical benefit than the case with mirrors on both faces. This is due to the optical coupling of the rear mirror to light between 1000 and 1160 nm incident on the front face. At these wavelengths, sunlight is not completely absorbed in a single pass. Without a rear mirror, this light may be reflected back into the cell by the rear air/glass interface, increasing carrier generation. With the rear mirror, which is an ideal antireflection coating at these wavelengths, all sunlight that is not trapped by total internal reflection exits the module, decreasing the possible amount of carrier generation. This detrimental optical coupling is also present for 1000−1160 nm light incident on the rear face, but its effect on optical benefit is small under most operating conditions (<0.05% absolute).

Including a coating with antireflection properties above the bandgap typically leads to elevated operating temperatures due to the additional parasitic and photothermal losses. Here, this temperature rise is outweighed by the sub-bandgap reflection, even though the baseline is partially transparent to sub-bandgap radiation (Figure 1c). The inclusion of an idealized spectrally selective mirror results in a 1.1% thermal benefit under front side AM1.5G irradiance, corresponding to a cell cooling of 2.7 °C. As the rear irradiance increases, including a mirror at the rear air/glass interface further increases the thermal benefit due to the increase in total sub-bandgap power reflected from the module. Omission of this rear mirror results in a slight decrease in thermal benefit with increasing rear irradiance. This arises from the optical coupling of the front mirror to the light incident from the rear face; while the unity sub-bandgap reflection of the mirror prevents sub-bandgap parasitic absorption of light incident on the front face, it also traps sub-bandgap radiation incident from the rear, increasing the parasitic absorption of light.

To study how realistic mirrors perform under real-world conditions, four- and six-layer spectrally selective mirrors were designed for a single-axis tracking system in Golden, CO, over the standard "light soil" ground coverage defined in the AM1.5G specifications.[26] Mirror compositions can be found in section S5. These low-complexity designs require significantly fewer deposition steps than many spectrally selective mirror designs previously proposed that are tens of layers thick.[17−19,28,29] Notably, the low number of degrees of freedom in these low-complexity designs forced the front and rear mirrors to converge to the same solution, even though they were independently optimized. The mirrors' reflection spectra relative to a bare air/glass interface are shown in Figures 2a and 2b. As expected, both designs exhibit above-bandgap antireflection and sub-bandgap enhanced reflection. While some angular dependence of the mirror's spectral response is unavoidable in these low-complexity designs, the mirrors largely maintain the angle of incidence invariance seen for optimized mirrors designed for fixed axis systems.[18,19] A standard 99 nm thick antireflection coating (ARC)[30] was also simulated as a reference (Figure S7).

https://doi.org/10.1021/acsaem.1c01236
ACS Appl. Energy Mater. 2021, 4, 5397−5402

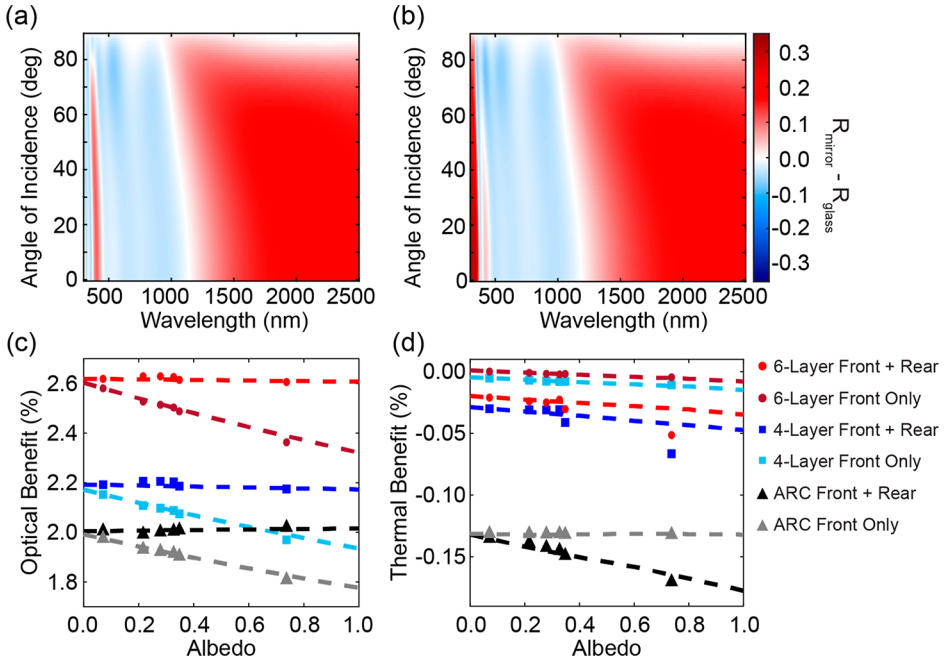

Figure 2. Angle-resolved reflection spectra of the (a) four- and (b) six-layer mirrors relative to glass. (c) Optical and (d) thermal benefits of the spectrally selective mirrors and traditional ARC when placed on either the front only or both air/glass interfaces. Mirror benefits calculated with spectral albedo are denoted by points while wavelength independent albedo is denoted in dashed lines.

We then considered the spectral albedo of other ground coverages by modeling six real ground albedos in the SMARTS2 library (asphalt, green grass, light soil, concrete, white sand, and snow)[22,23] as well as wavelength-independent albedos ranging from perfectly absorbing to perfectly reflecting ground (Figure S8). Figures 2c and 2d display the optical and thermal mirror benefit for each ground coverage/mirror combination. The dashed lines represent results from simulations with wavelength-independent albedo, and the points represent the results of the simulations with spectral ground albedos, which were converted to a single value by using eq 1.

$$\text{albedo}_{WI} = \int \text{albedo}(\lambda)\text{AM1.5G}(\lambda)\, d\lambda / \int \text{AM1.5G}(\lambda)\, d\lambda \quad (1)$$

Figure 2c shows that when mirrors are placed only on the front face, the optical benefit decreases with increasing ground albedo due to the increasing percentage of rear irradiance (Figures S9 and S10). This optical benefit can be preserved, however, with the inclusion of a rear mirror. The added benefit of the rear mirror also increases due to the increasing amount of rear irradiance. Finally, Figure 2c highlights the four- and six-layer mirrors' superior above-bandgap antireflection compared to the more traditional ARC, as observed by the constant 0.2% and 0.6% respective optical benefit increases.

Figure 2d shows the effect of different types of ground cover on the thermal benefit. The mirrors block ~20% of sub-bandgap radiation, which is not enough to generate significant module cooling but is sufficient to compensate for the increased heat generation that accompanies above-bandgap antireflection. Thus, these mirrors act as thermally aware antireflection coatings, thermally outperforming traditional ARCs while providing additional optical benefit. In contrast to the results shown in Figure 1c, the use of imperfect sub-bandgap reflectors on both faces of the module has an adverse effect on thermal performance. We attribute this to the trapping of sub-bandgap light admitted through the front face of the module. Replacing the rear mirror with a traditional ARC can eliminate the light trapping effect, resulting in a reduced thermal penalty at low levels of rear irradiance at the cost of a reduced optical benefit (Figure S11). These counteracting effects cause the overall system benefit change to be within the uncertainty of the calculations when the rear mirror is replaced with a single layer ARC under most realistic conditions.

The spectral nature of the ground did not significantly affect the optical and thermal benefits for any of the mirror/ground configurations, with the exception of the increased thermal penalty when the spectrally selective mirrors were placed on both faces and over snow (albedo_{WI} = 0.74). Snow's spectral albedo has high above-bandgap and low sub-bandgap reflectance and thus acts as a sub-bandgap filter for light incident on the rear face. The rear spectrally selective mirrors can still provide above-bandgap antireflection but are no longer able to compensate for the increases in cell parasitic and photothermal losses with sub-bandgap reflection, as observed by the increase in thermal penalty.

To study the effects of changing geographic location, the single-axis tracking field, originally in Golden, CO, was modeled in 11 additional US cities with varying climates ranging from Anchorage, AL, to Honolulu, HI (Table S3). As the geographic location changes, several important factors affect the module's thermal and optical environments (Figure S12). First, varying location affects the intensity and spectral distribution of light incident on the solar array. Additionally, the angular distribution of light received on the front face varies with latitude. As latitude increases, the single-axis tracking modules generally receive irradiance at higher angles of incidence. Lastly, each location has different temperatures and wind speeds, which affect the radiative and convective heat transfer of the modules with the surroundings.

https://doi.org/10.1021/acsaem.1c01236
ACS Appl. Energy Mater. 2021, 4, 5397−5402

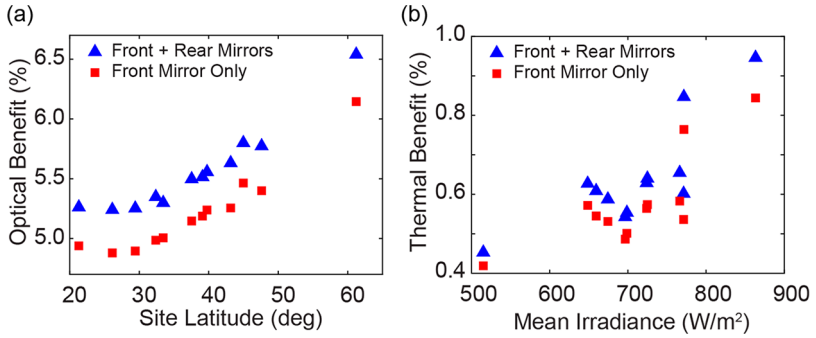

Figure 3. Location effects on mirror benefit for ideal mirrors. (a) Optical benefit vs site latitude. (b) Thermal benefit as a function of the contraharmonic mean irradiance incident on the module.

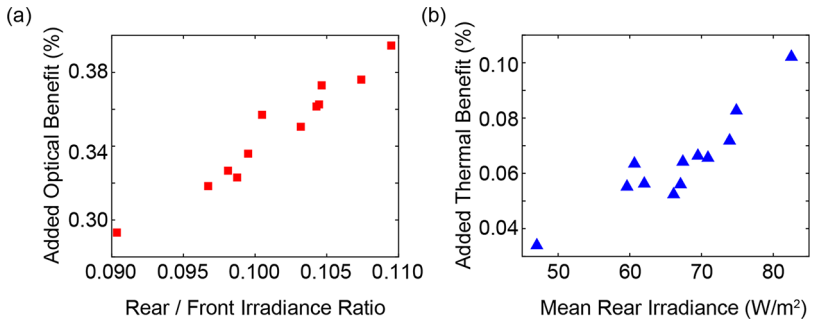

Figure 4. Location effects on rear mirror added benefit for ideal mirrors. (a) Rear mirror added optical benefit vs rear/front irradiance ratio. (b) Rear mirror added thermal benefit as a function of the contraharmonic mean irradiance incident on the module's rear face.

Figure 3 shows the optical and thermal benefits that are predicted for ideal mirrors in these different locations. As the latitude increases, the optical benefit increases because the ideal above-bandgap antireflection becomes increasingly beneficial at large angles of incidence. An uncoated air/glass interface has ∼4% reflectance at normal incidence, placing an upper limit for optical benefit at normal incidence (see 0 rear irradiance condition of Figure 1b). As the incident light moves off normal, air/glass reflection increases as dictated by Fresnel's equations, increasing the potential benefit of an omnidirectional antireflection coating.

The thermal benefit in the idealized case is correlated with the contraharmonic mean irradiance incident on the module, as sub-bandgap reflection cooling is directly linked to the amount of incident sub-bandgap radiation. However, there is some scatter in the relationship, as the thermal benefit is also a function of ambient temperature and wind speed that affect the ratio of convective to radiative heat transfer. The contraharmonic mean irradiance is defined by eq 2:

$$\mathrm{Irr}_{\mathrm{mean}} = \frac{\sum_t \left\{ \sum_\theta \int [\mathrm{Irr}_{\mathrm{Front}}(t, \theta, \lambda) + \mathrm{Irr}_{\mathrm{Rear}}(t, \theta, \lambda)]\, \mathrm{d}\lambda \right\}^2}{\sum_{t,\theta} \int [\mathrm{Irr}_{\mathrm{Front}}(t, \theta, \lambda) + \mathrm{Irr}_{\mathrm{Rear}}(t, \theta, \lambda)]\, \mathrm{d}\lambda} \tag{2}$$

where $\mathrm{Irr}_{\mathrm{Front,Rear}}(t,\theta,\lambda)$ is the time, angle, and wavelength resolved irradiance incident on the front or rear face found by using our view factor model (section S3). The contraharmonic mean was used over the more traditional arithmetic mean to exclude nighttime hours from the averaging. The maximum thermal benefit of 0.95% occurred in the sunniest location tested, Phoenix, AZ, with ideal mirrors located at both front and rear air/glass interfaces. This corresponds to a module temperature reduction of ∼2.4 °C and provides an approximate upper limit for sub-bandgap reflective cooling for bPVs under realistic conditions. Figure S13 shows the complementary data set.

The additional optical benefit provided by the rear mirror was found to be directly proportional to the rear/front irradiance ratio (Figure 4a). The *y*-axis of Figure 4a refers to the power increase from to the above-bandgap antireflection when the rear mirror is added. The rear mirror added thermal benefit had the opposite trend, linearly deceasing with rear/front irradiance ratio (Figure S14). To understand these opposite trends, it is important to consider the differing factors that lead to optical and thermal mirror benefits. The optical benefit a mirror provides is proportional to the *percentage* of above-bandgap photons that are transmitted into the cell by the improved antireflection coating. The thermal benefit, on the other hand, is proportional to the *total* sub-bandgap power blocked by the mirror. Even though the percentage contribution decreases, the magnitude of rear irradiance increases with total irradiance, resulting in the positive linear correlation between mean rear irradiance and added thermal benefit shown in Figure 4b. A similar data set for the four- and six-layer mirrors is shown in Figure S15.

As increasing numbers of bifacial modules are deployed, light management strategies are becoming ever more important. This Letter investigates how spectrally selective mirrors placed either at the front interface or both the front and rear air/glass interfaces of a bifacial PERC module can be used to enhance energy yield. We find that placing mirrors only at the front interface is sufficient for low rear irradiance conditions, but the added benefit of a rear spectrally selective mirror grows as the ground's albedo increases, with the spectral nature of the ground albedo only playing a minor role. Coupling between mirrors for long-wavelength light leads to detrimental effects such as sub-bandgap light trapping and above-bandgap light rejection, but these effects are secondary

https://doi.org/10.1021/acsaem.1c01236
ACS Appl. Energy Mater. 2021, 4, 5397−5402

compared to the benefit the mirrors provided for all but the limiting cases. Lastly, the mirror benefit was also tested as a function of geographic location. As site latitude moves away from the equator, the optical benefit potential increases due to an increase in off-normal front irradiance. The thermal benefit depends not only on the site's sunniness and absolute rear irradiance but also on varying convective cooling due to differences in wind.

■ ASSOCIATED CONTENT

Supporting Information

The Supporting Information is available free of charge at https://pubs.acs.org/doi/10.1021/acsaem.1c01236.

> Test cell characterization, simulation methodology, low-complexity mirror designs, ARC reflectance, ground albedos, annually averaged irradiance and angle distributions, optical and thermal benefits of using a spectrally selective mirror−ARC combination, geographic location summary, complementary data for Figures 3 and 4, low-complexity mirror benefits vs location (PDF)

■ AUTHOR INFORMATION

Corresponding Author

Vivian E. Ferry − *Department of Chemical Engineering and Materials Science, University of Minnesota, Minneapolis, Minnesota 55455, United States;* orcid.org/0000-0002-9676-6056; Email: veferry@umn.edu

Authors

Bryan M. Cote − *Department of Chemical Engineering and Materials Science, University of Minnesota, Minneapolis, Minnesota 55455, United States*

Ian M. Slauch − *Department of Chemical Engineering and Materials Science, University of Minnesota, Minneapolis, Minnesota 55455, United States*

Michael G. Deceglie − *National Renewable Energy Laboratory, Golden, Colorado 80401, United States*

Timothy J Silverman − *National Renewable Energy Laboratory, Golden, Colorado 80401, United States*

Complete contact information is available at: https://pubs.acs.org/10.1021/acsaem.1c01236

Notes

The authors declare no competing financial interest.

■ ACKNOWLEDGMENTS

The authors thank Dr. Silvana Ayala for helpful discussions. This material is based upon work supported by the U.S. Department of Energy Office of Energy Efficiency (EERE) under the Solar Energy Technologies Office Award DE-EE0008542. Part of this work was performed with equipment supported by funding from the National Science Foundation through the UMN MRSEC under Award DMR-2011401. The authors acknowledge the Minnesota Supercomputing Institute (MSI) at the University of Minnesota for providing resources that contributed to the research results reported within this paper. This work was authored in part by Alliance for Sustainable Energy, LLC, the manager and operator of the National Renewable Energy Laboratory for the U.S. Department of Energy (DOE) under Contract DE-AC36-08GO28308. Funding was provided by the U.S. Department of Energy's Office of Energy Efficiency and Renewable Energy (EERE) under Solar Energy Technologies Office (SETO) Agreement 30312 and by the Engineering Research Center Program of the National Science Foundation and under NSF Cooperative Agreement EEC-1041895. The views expressed herein do not necessarily represent the views of the U.S. Department of Energy or the United States government.

■ REFERENCES

(1) Gu, W.; Ma, T.; Ahmed, S.; Zhang, Y.; Peng, J. A Comprehensive Review and Outlook of Bifacial Photovoltaic (BPV) Technology. *Energy Convers. Manage.* **2020**, *223*, 113283.

(2) Chiodetti, M. *Bifacial PV Plants: Performance Model Development and Optimization of Their Configuration*. Master's Thesis; KTH Royal Institute of Technology: Stockholm, Sweden, 2015.

(3) Fischer, M.; Wang, Q.; Woodhouse, M.; Herritsch, S.; Trube, J. *International Technology Roadmap for Photovoltaic (ITRPV)*, 11th ed.; VDMA Photovoltaic Equipment: Frankfurt, Germany, 2020.

(4) Dullweber, T.; Kranz, C.; Peibst, R.; Baumann, U.; Hannebauer, H.; Fülle, A.; Steckemetz, S.; Weber, T.; Kutzer, M.; Müller, M.; Fischer, G.; Palinginis, P.; Neuhaus, H. PERC+: Industrial PERC Solar Cells with Rear Al Grid Enabling Bifaciality and Reduced Al Paste Consumption. *Prog. Photovoltaics* **2016**, *24* (12), 1487−1498.

(5) Sun, X.; Khan, M. R.; Deline, C.; Alam, M. A. Optimization and Performance of Bifacial Solar Modules: A Global Perspective. *Appl. Energy* **2018**, *212*, 1601−1610.

(6) Pelaez, S. A.; Deline, C.; Greenberg, P.; Stein, J. S.; Kostuk, R. K. Model and Validation of Single-Axis Tracking With Bifacial PV. *IEEE J. Photovolt.* **2019**, *9* (3), 715−721.

(7) Shoukry, I.; Libal, J.; Kopecek, R.; Wefringhaus, E.; Werner, J. Modelling of Bifacial Gain for Stand-Alone and in-Field Installed Bifacial PV Modules. *Energy Procedia* **2016**, *92*, 600−608.

(8) Lamers, M. W. P. E.; Özkalay, E.; Gali, R. S. R.; Janssen, G. J. M.; Weeber, A. W.; Romijn, I. G.; Van Aken, B. B. Temperature Effects of Bifacial Modules: Hotter or Cooler? *Sol. Energy Mater. Sol. Cells* **2018**, *185*, 192−197.

(9) Sun, X.; Silverman, T. J; Zhou, Z.; Khan, M. R.; Bermel, P.; Alam, M. A. Optics-Based Approach to Thermal Management of Photovoltaics: Selective-Spectral and Radiative Cooling. *IEEE J. Photovolt.* **2017**, *7* (2), 566−574.

(10) Dupré, O.; Vaillon, R.; Green, M. A. Thermal Issues in Photovoltaics and Existing Solutions. In *Thermal Behavior of Photovoltaic Devices: Physics and Engineering*; Dupré, O., Vaillon, R., Green, M. A., Eds.; Springer International Publishing: Cham, 2017; pp 1−28.

(11) Silverman, T. J; Deceglie, M. G.; Subedi, I.; Podraza, N. J.; Slauch, I. M.; Ferry, V. E.; Repins, I. Reducing Operating Temperature in Photovoltaic Modules. *IEEE Journal of Photovoltaics* **2018**, *8* (2), 532−540.

(12) Bahaidarah, H.; Subhan, A.; Gandhidasan, P.; Rehman, S. Performance Evaluation of a PV (Photovoltaic) Module by Back Surface Water Cooling for Hot Climatic Conditions. *Energy* **2013**, *59*, 445−453.

(13) Alami, A. H. Effects of Evaporative Cooling on Efficiency of Photovoltaic Modules. *Energy Convers. Manage.* **2014**, *77*, 668−679.

(14) Emam, M.; Ahmed, M. Cooling Concentrator Photovoltaic Systems Using Various Configurations of Phase-Change Material Heat Sinks. *Energy Convers. Manage.* **2018**, *158*, 298−314.

(15) Simpson, L. J.; Woods, J.; Valderrama, N.; Hill, A.; Vincent, N.; Silverman, T. Passive Cooling of Photovoltaics with Desiccants. In *2017 IEEE 44th Photovoltaic Specialist Conference (PVSC); Washington, DC*, 2017; pp 1893−1897.

(16) Gentle, A. R.; Smith, G. B. Is Enhanced Radiative Cooling of Solar Cell Modules Worth Pursuing? *Sol. Energy Mater. Sol. Cells* **2016**, *150*, 39−42.

(17) An, Y.; Sheng, C.; Li, X. Radiative Cooling of Solar Cells: Opto-Electro-Thermal Physics and Modeling. *Nanoscale* **2019**, *11* (36), 17073−17083.

(18) Slauch, I. M.; Deceglie, M. G.; Silverman, T. J; Ferry, V. E. Spectrally Selective Mirrors with Combined Optical and Thermal Benefit for Photovoltaic Module Thermal Management. *ACS Photonics* **2018**, *5* (4), 1528−1538.
(19) Slauch, I. M.; Deceglie, M. G.; Silverman, T. J; Ferry, V. E. Model for Characterization and Optimization of Spectrally Selective Structures to Reduce the Operating Temperature and Improve the Energy Yield of Photovoltaic Modules. *ACS Appl. Energy Mater.* **2019**, *2* (5), 3614−3623.
(20) Zhou, Z.; Jiang, Y.; Ekins-Daukes, N.; Keevers, M.; Green, M. A. Optical and Thermal Emission Benefits of Differently Textured Glass for Photovoltaic Modules. *IEEE J. Photovolt.* **2021**, *11* (1), 131−137.
(21) McIntosh, K. R.; Abbot, M.; Sudbury, B. *SunSolve*; PVLighthouse: 2020.
(22) Gueymard, C. Simple Model for the Atmospheric Radiative Transfer of Sunshine (SMARTS2) Algorithms and Performance Assessment, 1995; p 84.
(23) Gueymard, C. A. Parameterized Transmittance Model for Direct Beam and Circumsolar Spectral Irradiance. *Sol. Energy* **2001**, *71* (5), 325−346.
(24) Marion, B.; MacAlpine, S.; Deline, C.; Asgharzadeh, A.; Toor, F.; Riley, D.; Stein, J.; Hansen, C. A Practical Irradiance Model for Bifacial PV Modules. In *2017 IEEE 44th Photovoltaic Specialist Conference (PVSC)*; IEEE: Washington, DC, 2017; pp 1537−1542.
(25) Silverman, T. J; Deceglie, M. G. *PV TOMCAT*, ver. 1, 2020, https://github.com/NREL/PV_TOMCAT.
(26) ASTM G173-03(2020). *Standard Tables for Reference Solar Spectral Irradiances: Direct Normal and Hemispherical on 37° Tilted Surface*; ASTM International: West Conshohocken, PA, 2020.
(27) Deline, C.; MacAlpine, S.; Marion, B.; Toor, F.; Asgharzadeh, A.; Stein, J. S. Assessment of Bifacial Photovoltaic Module Power Rating Methodologies—Inside and Out. *IEEE J. Photovolt.* **2017**, *7* (2), 575−580.
(28) Li, W.; Shi, Y.; Chen, K.; Zhu, L.; Fan, S. A Comprehensive Photonic Approach for Solar Cell Cooling. *ACS Photonics* **2017**, *4* (4), 774−782.
(29) Zhao, B.; Hu, M.; Ao, X.; Xuan, Q.; Pei, G. Comprehensive Photonic Approach for Diurnal Photovoltaic and Nocturnal Radiative Cooling. *Sol. Energy Mater. Sol. Cells* **2018**, *178*, 266−272.
(30) Vogt, M. R. Development of Physical Models for the Simulation of Optical Properties of Solar Cell Modules. PhD. Dissertation, Leibniz University, Hannover, Germany, 2015.

https://doi.org/10.1021/acsaem.1c01236
ACS Appl. Energy Mater. 2021, 4, 5397−5402